PROCEEDINGS OF SPIE

In vivo imaging of cell nuclei by photoacoustic microscopy without staining

Da-Kang Yao, Ruimin Chen, Konstantin Maslov, Qifa Zhou, Lihong V. Wang

SPIE.

In Vivo Imaging of Cell Nuclei by Photoacoustic Microscopy without Staining

Da-Kang Yao[1], Ruimin Chen[2], Konstantin Maslov[1], Qifa Zhou[2], and Lihong V. Wang[1, *]

[1]Optical Imaging Laboratory, Department of Biomedical Engineering, Washington University in St. Louis, One Brookings Drive, St. Louis, Missouri 63130, USA
[2]Department of Biomedical Engineering, University of Southern California, 1042 Downey Way, Los Angeles, CA 90089, USA
*Corresponding author: lhwang@biomed.wustl.edu

ABSTRACT

Ultraviolet photoacoustic microscopy (UVPAM) can image cell nuclei in vivo with high contrast and resolution noninvasively without staining. Here, we used UV light at wavelengths of 210-310 nm for excitation of DNA and RNA to produce photoacoustic waves. We applied the UVPAM to *in vivo* imaging of cell nuclei in mouse skin, and obtained UVPAM images of the unstained cell nuclei at wavelengths of 245-282 nm as ultrasound gel was used for acoustic coupling. The largest ratio of contrast to noise was found for the images of cell nuclei at a 250 nm wavelength.

Keywords: DNA, RNA, label-free, histology, cancer diagnosis, UV light

1. INTRODUCTION

Imaging of cell nuclei plays an important role in cancer diagnosis. The nuclei in cancer cells are different from normal nuclei in morphology. For example, two morphological characteristics of cancer cell nuclei are large size and mitotic figure [1]. Besides eccentric nuclear morphology, irregular distribution of cell nuclei is characteristic of cancer. Right now, these characteristics are applied as the gold standard by pathologists to determine cancer grade and evaluate prognosis [2]. Classical imaging of cell nuclei in tissues goes through a complicated histological process, including tissue biopsying, processing, embedding, sectioning, and staining before imaging with optical microscopy [3]. Without staining, *in vivo* imaging of cell nuclei has been achieved by the ultraviolet photoacoustic microscopy (UV-PAM) [4].

UV-PAM is a new photoacoustic imaging technique capable of specially imaging cell nuclei in live tissue. In UV-PAM, a pulsed laser beam of ultraviolet light (UV) is focused into the tissue. DNA and RNA, two major components of cell nuclei, strongly absorb UV light at wavelengths around 260 nm [5, 6]. The absorbed light is converted into heat in the nuclei. Thermoelastic expansion generates ultrasonic waves, which are detected as photoacoustic signals by a focused ultrasonic transducer. The photoacoustic signals are then processed to produce a nuclear image with positive contrast. Using light with a wavelength of 266 nm, we have demonstrated that UV-PAM can generate high contrast images of cell nuclei [4]. Besides the 266 nm wavelength, various UV wavelengths are available within the absorption spectra of DNA and RNA. In order to find the optimal UV-PAM wavelength, we imaged cell nuclei *in vivo* at various wavelengths, using a UV-PAM system equipped with a tunable laser.

2. MATERIALS AND METHODS

2.1 Animal Preparation

Six female athymic nude mice (Harlan Laboratories, Indianapolis, IN) were used for *in vivo* imaging. The mice were anesthetized with 1% isoflurane (Butler Animal Health Supply, Dublin, OH) delivered in pure oxygen (Airgas, St. Louis,

MO) at a flow rate of 0.5 L/min. Before imaging, the mouse ear skin was gently washed three times using distilled water. After imaging, the mice recovered in ten minutes. All experimental animal procedures were carried out in conformity with the laboratory animal protocol of the Animal Studies Committee of Washington University in St. Louis.

2.2 Ultraviolet Photoacoustic Microscopy

A detailed description of the original UV-PAM system was reported previously [4]. In order to investigate the optimal wavelength for *in vivo* photoacoustic imaging of cell nuclei, we equipped the UV-PAM system with an OPO laser system (NT242-SH, Altos Photonics, Bozeman, MT) that provides a wavelength tuning range from 210 to 2300 nm [7]. Figure 1 is a schematic of the improved UV-PAM system. A pulsed UV laser beam with a pulse width of 5 ns is emitted from the tunable laser system at a repetition rate of 1 kHz. After being attenuated by a neutral density filter (NDC-50C-4M, Thorlabs, Newton, NJ), the laser beam is focused by a 100-mm-focal-length off-axis parabolic mirror (50338AL, Newport, Irvine, CA), and then spatially filtered by a 25 µm diameter pinhole (910PH-25, Newport). The beam is refocused into a water tank by a 0.1 NA objective lens (LA4280, Thorlabs), passes through a focused ring ultrasonic transducer (50 MHz central frequency, 7 mm focal length), and penetrates a 25 µm thick polyethylene membrane before focusing along the z axis to an object. The ultrasonic transducer is coaxially aligned with the objective lens to a common focus. The polyethylene membrane forms an optical window on the bottom of the water tank and maintains acoustic coupling. The laser pulse energy behind the membrane is measured by a digital power meter (PM100D, Thorlabs) with a silicon photodiode sensor (S120VC, Thorlabs). The water tank and the specimen are mounted on a translation stage (PT1, Thorlabs), which is vertically installed on a two-dimensional scanning stage (Micos USA, Irvine, CA) for manual focusing of the specimen. While the scanning stage performs raster scanning with a step size of 0.62 µm in the horizontal plane (x-y plane), photoacoustic signals are detected by the ultrasonic transducer, amplified by an amplifier (ZFL-500LN, Mini-Circuits, Branson, MO), and collected by a computer through a 12-bit, 200 MHz digitizer (NI PCI-5124, National Instruments, Austin, TX).
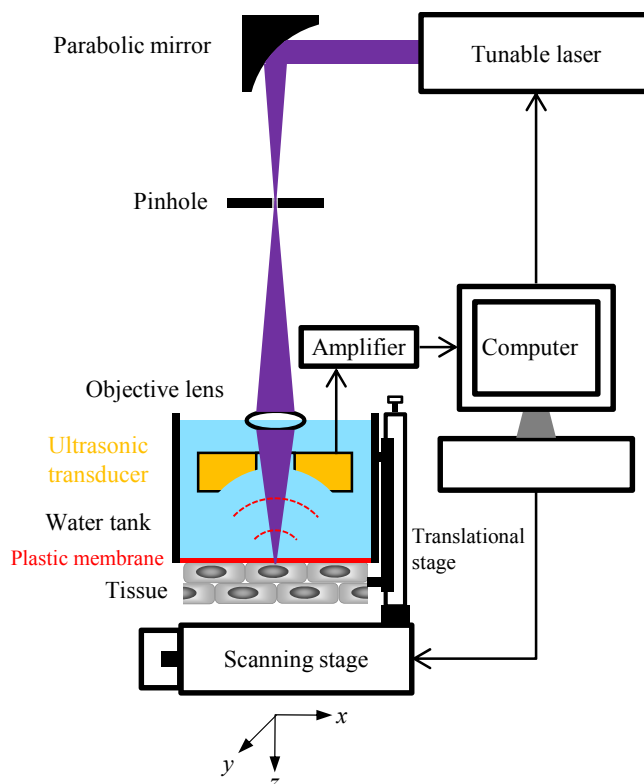

Figure 1. Schematic of the ultraviolet photoacoustic microscopy system.

240 nm 242 nm 245 nm

248 nm 250 nm 251 nm

252 nm 255 nm 260 nm

266 nm 270 nm 280 nm

282 nm 285 nm 290 nm

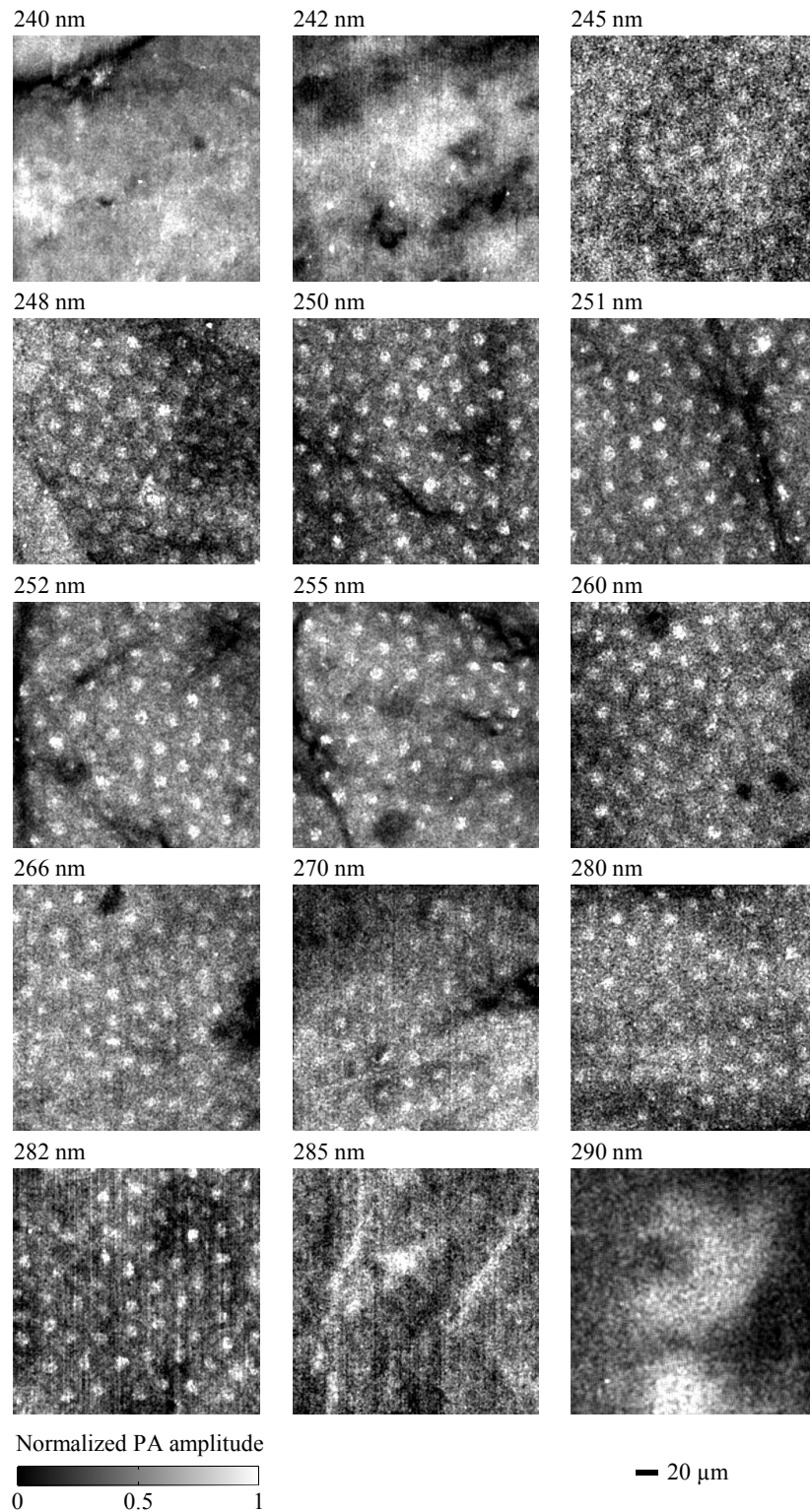Normalized PA amplitude

0　　　　0.5　　　　1

━ 20 μm

Figure 2. *In vivo en face* photoacoustic images of the skin of mouse ears in the form of maximum amplitude projection (MAP). Ultrasound gel was used for acoustic coupling. Laser pulse energy was 20 nJ. PA, photoacoustic.

RESULTS

3.1 Wavelength range

We imaged cell nuclei *in vivo* in the ear skin of the mice using various wavelengths. An anesthetized mouse was held by a custom-made stereotaxic imaging stage. After the imaging stage was mounted on the translational stage, a mouse ear was flat placed on a plastic plate immobilized on the imaging stage. A film of ultrasound gel was used between the image window and the mouse ear. During the preview scanning, we adjusted the translational stage upward until a clear B-scan image was observed. Then, we scanned the ear skin with laser pulse energy of 20 nJ at wavelengths ranging from 210 to 310 nm. We repeated the experiments twice at wavelengths of 245, 248, 250, 251, 252, 255, 260, 266, 270, 280, and 282 nm. Both experiments yielded identifiable images of cell nuclei with positive contrast. Typical images are shown in Fig. 2. For wavelengths of 210, 220, 230, 240, 242, 285, 290, 300, and 310 nm, we repeated imaging experiments two to four times, but did not obtain any identifiable image of cell nuclei. Typical images of mouse ear skin acquired at wavelengths of 240, 242, 285, and 290 nm are shown in Fig. 2. All of these images show that wavelengths ranging from 245 to 282 nm are applicable to *in vivo* photoacoustic imaging of unstained cell nuclei as ultrasound gel is used as a coupling medium.

3.2 Optimal wavelength

We examined the signal-to-noise ratio (SNR) and the contrast-to-noise ratio (CNR) of the photoacoustic images of cell nuclei. All images were acquired with laser pulse energy of 20 nJ. The mean intensity of the image of a single cell nucleus was obtained by averaging the amplitude within a square window of 10×10 pixels in the image of the cell nucleus. In order to analyze background intensity, we chose a large square window of 30×30 pixels and a small square window of 20×20 pixels, both of which were concentric with the single nuclear image. The large window did not cover neighboring nuclei, and the small window totally covered the single nuclear image. Inside the larger window but outside the smaller one, we calculated the mean intensity of the background image surrounding the nuclear image. In order to measure image noise, we scanned the mouse ear using zero laser output in each experiment. A dummy photoacoustic image was formed with zero laser output and was used to compute the standard deviation of image intensity. For each wavelength between 245 and 282 nm, we calculated the SNR and CNR of the MAP images of 25 cell nuclei. After averaging, we obtained a correlation between image SNR and wavelength, as shown in Fig. 3(a), and a correlation between CNR and wavelength, as shown in Fig. 3(b). Both SNR and CNR significantly change with the wavelength, and each reaches its maximum at a wavelength of 250 nm. Particularly, the CNR at 250 nm was 2.6 times greater than that at 266 nm. Therefore, 250 nm was the optimal wavelength for *in vivo* photoacoustic imaging of unstained cell nuclei.
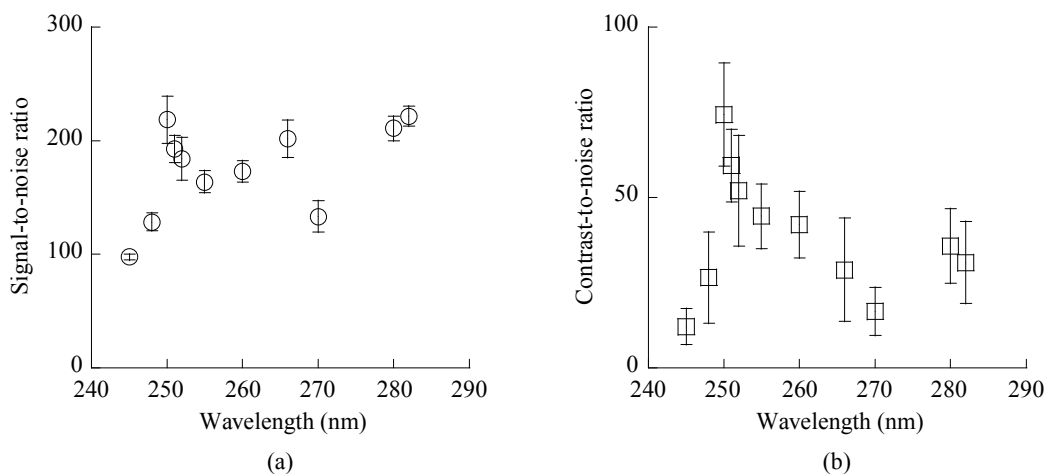

Figure 3. Correlations between *in vivo* photoacoustic image of cell nuclei and optical wavelength. At each wavelength, laser pulse energy was 20 nJ, and 25 cell nuclei were analyzed. (a) Plot of SNR (mean ± SD) of nuclear images versus wavelength. (b) Plot of CNR (mean ± SD) of nuclear images versus wavelength.

4. DISCUSSION

We applied UV-PAM to *in vivo* imaging of unstained cell nuclei at various wavelengths and obtained nuclear images with positive, specific, and high contrast. In UV-PAM, DNA and RNA are excited by UV light to generate photoacoustic signal. In animal cells, DNA and RNA are concentrated in cell nuclei. Once DNA and RNA are excited, strong photoacoustic signals come from cell nuclei, which results in the positive image contrast. Outside cell nuclei, weak UV absorption of protein only generates weak photoacoustic signals, which form a background. Comparing the background signals, the strong signals only come from cell nuclei, which results in the specific contrast for cell nuclei. The high image contrast results from a difference between strong light absorption of nucleic acids and weak absorption of protein, which reaches the maximum at a wavelength of 250 nm. In addition to UV-PAM, several other modern optical microscopy technologies have been explored for *in vivo* imaging of unstained cell nuclei, such as reflectance confocal microscopy [8-11], multiphoton microscopy [12-14], and third-harmonic generation microscopy [15, 16], However, reflectance confocal microscopy is difficult to provide specific image contrast for nuclei [8], multiphoton microscopy produces *in vivo* images of cell nuclei with negative contrast [13], and third harmonic generation microscopy generates nuclear images with low contrast [15].

We used a film of ultrasound gel with a thickness less than 30 μm for acoustic coupling. The film was between the plastic membrane on the bottom of water tank and mouse skin. We found that ultrasound gel significantly absorbed UV light at wavelengths between 210 and 310 nm. The UV absorption plus different film thickness could cause unrepeatable measurements of image SNR and CNR. In order to achieve repeatable measurement, we only put a tiny drop of ultrasound gel on the skin of mouse ears, and then filled the tank with water and let the plastic membrane on the tank bottom press the gel for 10 minutes (Fig. 1). Before imaging, we checked the film thickness using time-arrival photoacoustic signals. After the film thickness was less than the axial resolution of our UV-PAM system (29 μm), we started data collection for image construction.

5. CONCLUSIONS

After equipping a UV-PAM system with a tunable laser, we imaged cell nuclei in mouse skin *in vivo* at wavelengths ranging from 210 to 310 nm. Without staining, UV-PAM produced images of cell nuclei with specific, positive, and high contrast. The optimal wavelength is 250 nm for *in vivo* photoacoustic imaging of cell nuclei. Any wavelength between 245 and 282 nm can be used to produce *in vivo* images of cell nuclei. However, we did not obtain an identifiable nuclear image at wavelengths of 210, 220, 230, 240, 242, 285, 290, 300, and 310 nm.

ACKNOWLEDGEMENTS

REFERENCES

[1]   Zink, D., Fischer, A. H., and Nickerson, J. A., "Nuclear structure in cancer cells," Nat Rev Cancer. **4**(9), 677-687 (2004).
[2]   Connolly, J. L., et al., *Principles of Cancer Pathology*, in *Holland Frei cancer medicine 8*, W.K. Hong, et al., Editors. 2010, People's Medical Publishing House-USA: Shelton, CT.
[3]   Lester, S. C., *Manual of Surgical Pathology*. 2010, Philadelphia Saunders/Elsevier.
[4]   Yao, D. K., et al., "In vivo label-free photoacoustic microscopy of cell nuclei by excitation of DNA and RNA," Opt Lett. **35**(24), 4139-41 (2010).
[5]   Tataurov, A. V., You, Y., and Owczarzy, R., "Predicting ultraviolet spectrum of single stranded and double stranded deoxyribonucleic acids," Biophysical Chemistry. **133**(1-3), 66-70 (2008).

[6]   Fleck, A. and Begg, D., "The estimation of ribonucleic acid using ultraviolet absorption measurements," Biochimica et Biophysica Acta (BBA) - Nucleic Acids and Protein Synthesis. **108**(3), 333-339 (1965).

[7]   Savage, N., "Optical parametric oscillators," Nat Photon. **4**(2), 124-125 (2010).

[8]   Nehal, K. S., Gareau, D., and Rajadhyaksha, M., "Skin Imaging With Reflectance Confocal Microscopy," Seminars in Cutaneous Medicine and Surgery. **27**(1), 37-43 (2008).

[9]   Dwyer, P. J., et al., "Confocal reflectance theta line scanning microscope for imaging human skin in vivo," Opt Lett. **31**(7), 942-4 (2006).

[10]   Gonzalez, S. and Tannous, Z., "Real-time, in vivo confocal reflectance microscopy of basal cell carcinoma," J Am Acad Dermatol. **47**(6), 869-74 (2002).

[11]   White, W. M., et al., "Noninvasive imaging of human oral mucosa in vivo by confocal reflectance microscopy," Laryngoscope. **109**(10), 1709-17 (1999).

[12]   Masters, B. R., So, P. T., and Gratton, E., "Multiphoton excitation fluorescence microscopy and spectroscopy of in vivo human skin," Biophys J. **72**(6), 2405-12 (1997).

[13]   Wang, B. G., Konig, K., and Halbhuber, K. J., "Two-photon microscopy of deep intravital tissues and its merits in clinical research," J Microsc. **238**(1), 1-20 (2010).

[14]   Chunqiang, L., et al., "Multiphoton Microscopy of Live Tissues With Ultraviolet Autofluorescence," Selected Topics in Quantum Electronics, IEEE Journal of. **16**(3), 516-523 (2010).

[15]   Tsai, M. R., et al., "In vivo optical virtual biopsy of human oral mucosa with harmonic generation microscopy," Biomed Opt Express. **2**(8), 2317-28 (2011).

[16]   Chen, S. Y., Wu, H. Y., and Sun, C. K., "In vivo harmonic generation biopsy of human skin," J Biomed Opt. **14**(6), 060505 (2009).